Order-disorder induced magnetic structures of $FeMnP_{0.75}Si_{0.25}$

Matthias Hudl* and Per Nordblad
Department of Engineering Sciences, Uppsala University, Box 534, SE-751 21 Uppsala, Sweden

Torbjörn Björkman, Olle Eriksson, and Lennart Häggström
Department of Physics and Astronomy, Uppsala University, Box 516, SE-751 20 Uppsala, Sweden

Martin Sahlberg and Yvonne Andersson
Department of Materials Chemistry, Uppsala University, P.O. Box 538, SE-751 21, Uppsala, Sweden

Erna-Krisztina Delczeg-Czirjak
School of Industrial Engineering and Management, Royal Institute of Technology, SE-100 44 Stockholm, Sweden

Levente Vitos
Department of Physics and Astronomy, Uppsala University, Box 516, SE-751 20 Uppsala, Sweden and School of Industrial Engineering and Management, Royal Institute of Technology, SE-100 44 Stockholm, Sweden

(Received 26 July 2010; revised manuscript received 21 December 2010; published 15 April 2011)

We report on the synthesis and structural characterization of the magnetocaloric $FeMnP_{0.75}Si_{0.25}$ compound. Two types of samples (quenched and slowly cooled) were synthesized and characterized structurally and magnetically. We have found that minor changes in the degree of crystallographic order causes large changes in the magnetic properties. The slow-cooled sample, with a higher degree of order, is antiferromagnetic. The quenched sample has a net moment of 1.26 μ_B per formula unit and ferrimagnetic behavior. Theoretical calculations give rather large values for the Fe and Mn magnetic moments, both when occupied on the tetrahedral and the pyramidal lattice sites.

DOI: 10.1103/PhysRevB.83.134420 PACS number(s): 75.30.Sg, 71.23.−k, 75.30.Cr, 81.40.Rs

I. INTRODUCTION

Compounds based on Fe_2P gain increased interest due to a possible application in magnetocaloric refrigeration. Recent publications by Brück *et al.*,[1,2] Dagula *et al.*,[3] and Cam Thanh *et al.*[4] reported huge magnetocaloric effects close to room temperature in $FeMnP_{1-x}As_x$, $FeMnP_{0.5}As_{0.5-x}Si_x$, and $FeMnP_{1-x}Si_x$, respectively. The compound $FeMnP_{1-x}Si_x$ is of particular interest since it consists of nontoxic elements. One drawback of $FeMnP_{1-x}Si_x$ as regard applications is a strong thermal hysteresis when undergoing its first-order para- to ferromagnetic phase transition.

The Fe_2P compound has been intensely studied during the last five decades. Fe_2P crystallizes in a hexagonal structure with space group D^3_{3h} ($P\bar{6}2m$).[5] The iron atoms occupy two different crystal sites, the 3*f* site with four phosphorus atoms surrounding one iron atom (referred to as a type-I or tetrahedral site) and the 3*g* site with five phosphorus atoms surrounding one iron atom (referred to as a type-II or pyramidal site). The phosphorus atoms occupy two dissimilar sites: 2*c* (type I) and 1*b* (type II). Each Fe(1) site is surrounded by two P(1) and two P(2) atoms whereas Fe(2) is surrounded by four P(1) atoms and one P(2) atom (Fig. 1). As regards the magnetic properties Fe_2P undergoes a first-order para- to ferromagnetic phase transition with a Curie temperature of $T_C \approx 216$ K (see, e.g., Wäppling *et al.*,[6] Fujii *et al.*,[7] and Lundgren *et al.*[8]). It is worth noticing that prior to this investigation structural and magnetic studies on $(Fe_{1-y}Mn_y)_2P$ and $Fe_2P_{1-x}Si_x$ were published by Srivastava *et al.*[9] and Jernberg *et al.*[10] Due to its interesting magnetic properties, Fe_2P has also attracted theoretical interest, e.g., as revealed in Refs. 11 and 12. An explanation for the occurrence of a first-order transition in Fe_2P is given by Yamada and Terao.[13]

A tentative phase diagram for $FeMnP_{1-x}Si_x$ is suggested by Cam Thanh *et al.*[4] and indicates a phase transition from orthorhombic to hexagonal structure for a silicon content of approximately $x = 0.25$. In spite of many previous studies, the importance of the iron-to-manganese ratio as well as the distribution of those atoms within the Fe_2P structure remains unexplored. In our study the magnetic, structural, and electronic properties of the $FeMnP_{0.75}Si_{0.25}$ alloy have been investigated, using XRD, Mössbauer spectroscopy, and magnetic measurements combined with theoretical calculations. We observe a significant, but reversible, difference in the magnetic order depending on the heat treatment protocol. The change in the magnetic order is supposedly caused by the degree of crystallographic order of iron and manganese atoms.

II. EXPERIMENTAL DETAILS AND METHODS

The $FeMnP_{0.75}Si_{0.25}$ sample was prepared by a drop synthesis method using a high-frequency induction furnace.[14] The synthesis was done under argon atmosphere and temperatures of approximately 1350 °C. The raw sample was directly taken from the cooled melt and investigated by x-ray diffraction (XRD). Thereafter some phosphorus was added and the fabricated material was annealed for 10 days at 1000 °C. All subsequent heat treatments did not involve changes in the element composition.

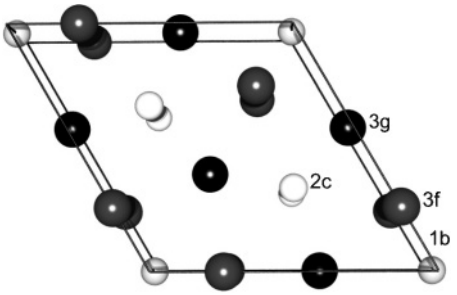

FIG. 1. Fe_2P structure with iron atom positions Fe(1) (dark gray) and Fe(2) (black), and phosphorus atom positions P(2) (light gray) and P(1) (white).

The XRD measurements were performed using a focusing Bragg-Brentano type powder diffractometer with Cu $K_{\alpha 1}$ radiation. The magnetic properties of all samples were investigated by means of magnetization measurements mainly using a commercial vibrating sample magnetometer (Quantum Design PPMS). Zero field cooled (ZFC) and field cooled (FC) measurement protocols for different fields were applied. The nomenclature of our samples is as follows: sample A, synthesized and quenched; sample B, annealed and slowly cooled; sample C, remelted and quenched; and sample D, remelted, annealed, and slowly cooled. The remelting was done using an arc melting furnace. Mössbauer spectra were recorded at room temperature and 77 K in the absorption mode with constant-acceleration drive and a ^{57}CoRh source. All samples A, B, C, and D were characterized by magnetization measurements; samples C and D were characterized by Mössbauer spectroscopy.

The electronic structure and total energy calculations were performed using the exact muffin-tin orbital method (EMTO)[15–18] in combination with the coherent potential approximation (CPA).[19,20] The EMTO method is an improved screened Korringa-Kohn-Rostoker method, where the one-electron potential is represented by large overlapping muffin-tin potential spheres. By using overlapping spheres, one describes more accurately the crystal potential, when compared to the conventional nonoverlapping muffin-tin approach. Further details about this method can be found in Refs. 15–18. The EMTO-CPA approach has been applied successfully in the theoretical study of random Fe-based alloys,[21] simple and transition metal alloys, and Hume-Rothery systems.

During the self-consistent calculations, we adopted the generalized gradient approximation of Perdew-Burke-Ernzerhof (PBE).[22] The total energy was computed via the full charge density technique[17,23] using the revised PBE for metallic bulk and surface systems (PBEsol).[24] With this approach, the deviation between the theoretical and experimental Wigner-Seitz radii is less than 0.1%.

Calculations were carried out for three different phases of $FeMn_{0.75}Si_{0.25}$. We considered two ordered phases: one with Mn atoms occupying the pyramidal (high moment) positions and one with Mn atoms occupying the tetrahedral (low moment) position. These structures are labeled as "Mn-pyramidal" and "Fe-pyramidal," respectively. In the third case, the Mn and Fe atoms are randomly distributed on the two Fe positions from the Fe_2P structure. This phase is referred to as "disordered." We assumed that all these phases have the hexagonal Fe_2P structure. The internal positions and lattice parameters were taken from Carlson *et al.*[25]

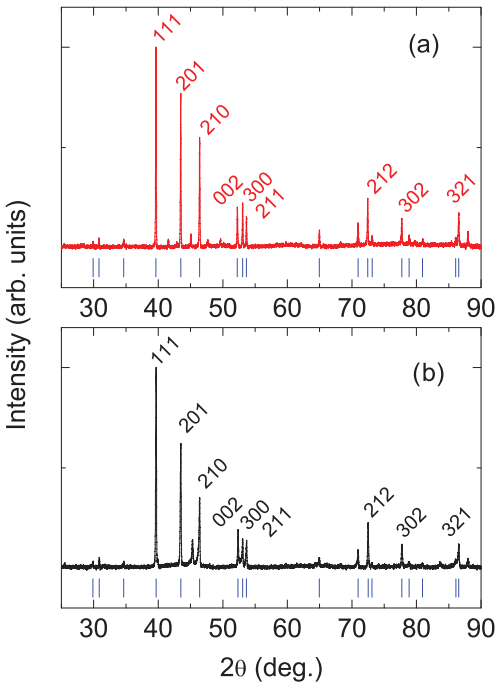

FIG. 2. (Color online) XRD patterns of (a) a slowly cooled and (b) a quenched $FeMnP_{0.75}Si_{0.25}$ sample. The blue lines mark the indexed peaks of the $FeMnP_{0.75}Si_{0.25}$ phase.

III. RESULTS AND DISCUSSION

A. X-ray diffraction

The x-ray data at room temperature yielded a hexagonal Fe_2P-type structure with unit cell dimensions $a = 5.973$ Å and $c = 3.498$ Å for the annealed, slowly cooled sample (B) [Fig. 2(a)]. The unit cell dimensions for the quenched sample were $a = 5.974$ Å and $c = 3.493$ Å. A weak cubic structure with cell dimension $a = 5.653$ Å was detected in the raw synthesized material (sample A), possibly of Fe_3Si type. In order to eliminate this fractional phase and to compensate a possible loss of phosphorus during the synthesis some phosphorus was added and the sample was annealed. After the annealing no trace of the Fe_3Si impurity phase could be deduced from the XRD data. A composition analysis carried out using an electron probe microanalyzer (WDS-EPMA) as well as energy dispersive spectroscopy (EDS) indicates an excess of iron to manganese with a Fe/Mn ratio of ~1.24 and a composition $Fe_{1.1(1)}Mn_{0.9(1)}P_{0.7(1)}Si_{0.2(1)}$ with the relative error bars derived after averaging over numerous measurements. In addition, our analysis revealed a new impurity phase, consisting of Fe and Si, which amounts to ~5% of our sample. This impurity phase is also observed in the XRD data set and was determined to be of FeSi type.

B. Mössbauer measurements

The quenched sample (C) and the slowly cooled sample (D) were probed by Mössbauer spectroscopy at room

temperature and 77 K. The distribution of iron atoms on the two inequivalent atomic positions Fe(1) and Fe(2) was investigated. In a Fe_2P structure the pyramidal Fe(2) site is preferentially occupied by the less electronegative atom and for small differences in the electronegativity by the atom with larger radius.[26] For FeMnP the tetrahedral site is occupied by iron and the pyramidal site by manganese.[9] In the case of $FeMnP_{0.75}Si_{0.25}$ with the same stoichiometric number of iron and manganese atoms one therefore would expect the iron atoms to be on the tetrahedral site and the manganese atoms on the pyramidal site. The spectral intensities from the Mössbauer analysis are modified from the site abundances due to the differences in the recoil free factor f and due to the so-called thickness effect. For Fe_2P different Debye temperatures, Θ_D**(**Fe(1)**)** = 383(6) K and Θ_D**(**Fe(2)**)** = 324(9) K,[10] have been found. Using these values the following f factors can be calculated: $f_1(300\ \mathrm{K}) = 0.75$, $f_2(300\ \mathrm{K}) = 0.67$, $f_1(77\ \mathrm{K}) = 0.89$, and $f_2(77\ \mathrm{K}) = 0.86$.

1. Room temperature Mössbauer spectra

In Fig. 3 the room temperature spectra are presented together with the fittings. The isomer shifts δ (mm/s) vs α-Fe at 295 K and electric quadrupole splittings Δ (mm/s) do not change significantly between the two spectra, being $(\delta, \Delta) =$ **(**0.27(1),0.24(1)**)** for Fe(1) and **(**0.55(1),0.53(1)**)** for Fe(2), respectively. These values are very close to the values found for pure hexagonal Fe_2P and in the hexagonal part of the system $Fe_{1-z}Mn_zP$.[9] The Fe(2) spectral intensity for the quenched sample (C) is found to 18(1)%, while the slowly cooled sample had an Fe(2) intensity of 13(1)%. In the present case the thickness effect for the two room temperature spectra can be assumed to be very similar since the total absorbance is almost the same (same Mössbauer thickness) and also due to that the lines emanating from Fe(1) and Fe(2) are not well

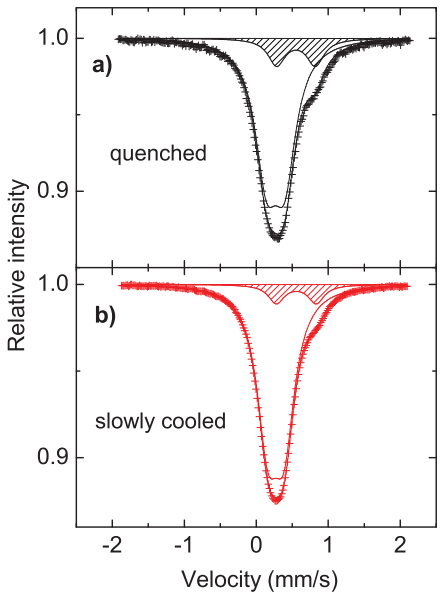

FIG. 3. (Color online) Room temperature Mössbauer spectra of $FeMnP_{0.75}Si_{0.25}$. Spectrum (a) corresponds to the quenched sample and spectrum (b) to the slowly cooled sample. The shaded doublets emanate from the pyramidal coordinated Fe(2) site.

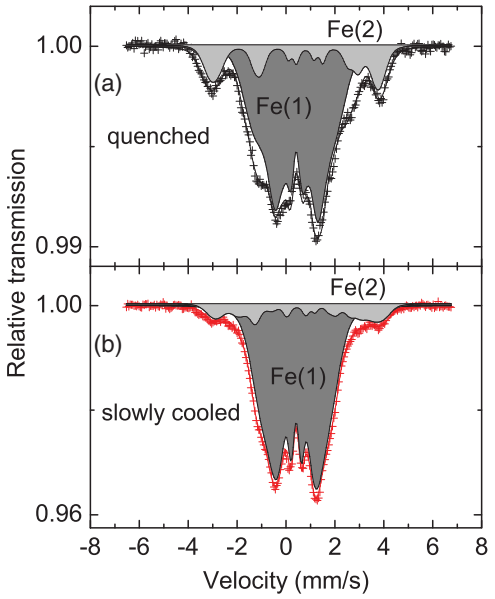

FIG. 4. (Color online) Mössbauer spectra recorded at 77 K for $FeMnP_{0.75}Si_{0.25}$, quenched and slowly cooled. The light gray subpattern emanates from Fe(2) atoms and the dark gray subpattern from Fe(1) atoms.

resolved. Modifying the spectral intensities by the difference in f factors gives the following Fe(2) site abundances: 20(1)% for sample C and 14(1)% for sample D.

2. Mössbauer spectra at 77 K

In Fig. 4 the spectra recorded in the magnetically ordered regime are displayed together with the fittings. For sample D one Fe(1) subspectrum and three Fe(2) subspectra were needed to get reasonable fits, while for sample C three Fe(1) and two Fe(2) subspectra were needed. The average isomer shift values for the Fe(1) and Fe(2) subspectra were 0.40(2) mm/s and 0.62(2) mm/s for both samples. These values are in good agreement with the values 0.41(1) and 0.66(1) found for pure Fe_2P.[10] The Fe(2) spectral intensities were found to be 20(1)% and 15(1)% for sample C and sample D, respectively. Modifying these spectral intensities due to the difference in the f factors gives the Fe(2) site abundances to be 20(1)% and 15(1)% for the samples C and D, respectively. The 295 K and 77 K site abundances are thus in good agreement. The magnetic hyperfine field distributions are presented in Fig. 5. In that figure the magnetic fields have been converted into magnetic moments using the conversion factor 10 T/μ_B found for pure Fe_2P by Eriksson *et al.*[11] The Fe(1) distribution sharpens markedly in the slowly cooled sample as compared to the quenched sample. The average Fe magnetic moments for Fe(1) and Fe(2) are 0.79 μ_B and 1.9 μ_B for the slowly cooled sample D and a bit larger 0.95 μ_B and 2.1 μ_B for the quenched sample C.

C. First-principles calculations

Figure 6 shows the calculated total energies as a function of the lattice parameter a (for fixed $c/a = 0.5894$) for three different phases: Mn-pyramidal, Fe-pyramidal, and disordered. We find that the Mn-pyramidal phase has the lowest energy

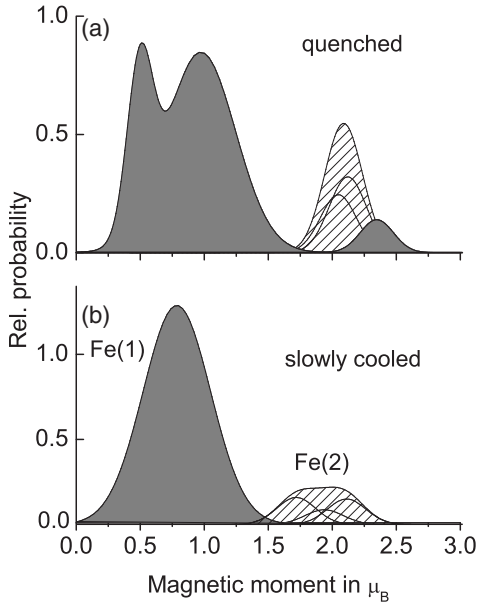

FIG. 5. The relative Fe magnetic moment population probabilities for $FeMnP_{0.75}Si_{0.25}$, quenched and slowly cooled samples. The conversion factor 10 T/μ_B has been used in converting the magnetic hyperfine fields into magnetic moments. Gray distributions emanate from Fe(1) and hatched distributions from Fe(2) atoms.

for all volumes (lattice parameters). This is in line with the experimental observation, namely that Mn atoms preferentially occupy the high-moment site. The energy difference between the considered phases is rather significant (5–10 mRy/site). The Mn-pyramidal phase has a shallow energy minimum for lattice constants around 5.95 Å, whereas our experimental value is 5.97 Å for the hexagonal $FeMnP_{0.75}Si_{0.25}$.

During the calculations the systems were kept in the high-moment state. This was possible for a >5.87 Å, but for

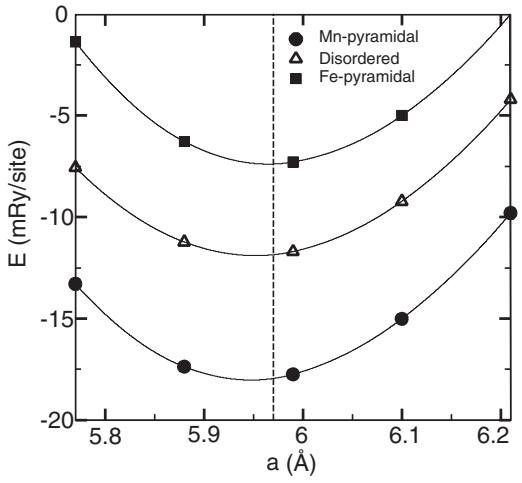

FIG. 6. Total energy per site for ordered and disordered phases of hexagonal $FeMnP_{0.75}Si_{0.25}$ as functions of the lattice parameter ($c/a = 0.5894$). The ordered phases correspond to the Mn atom occupying the pyramidal (high moment) and tetrahedral (low moment, labeled Fe pyramidal) positions, respectively. In the disordered phase the two positions are randomly occupied by Mn and Fe atoms. The dashed vertical line indicates the experimental a lattice parameter.

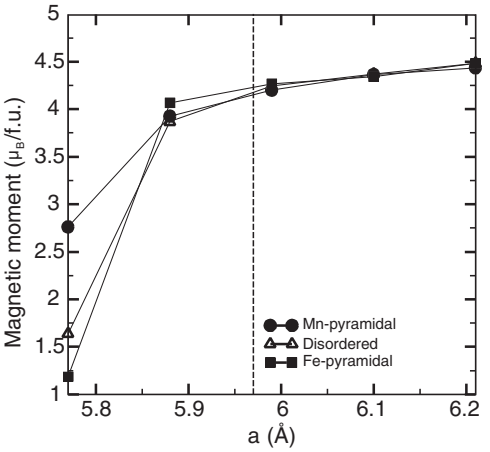

FIG. 7. Ordered magnetic moments per site for ordered and disordered phases of hexagonal $FeMnP_{0.75}Si_{0.25}$ as functions of the lattice parameter ($c/a = 0.5894$). The ordered phases, correspond to the Mn atom occupying the pyramidal (high moment) and tetrahedral (low moment, labeled Fe pyramidal) positions, respectively. In the disordered phase the two positions are randomly occupied by Mn and Fe atoms. The dashed-dotted vertical line indicates the experimental a lattice parameter.

a <5.87 Å a drop in the calculated total magnetic moments per formula unit can be seen (Fig. 7), due to what is known as the magnetovolume effect. Decreasing magnetism for lower volumes is a consequence of the competition between kinetic energy of the electron states, which is always lower for a spin-degenerate system, and the exchange energy, which is lower for a spin-polarized system. With decreasing volume the bandwidth becomes broader, and consequently the kinetic energy becomes the dominating term in the total energy. Hence, lower volumes favor the spin-degenerate state with vanishing magnetic moment. The competition between kinetic and exchange energy depends intricately on the details of the electronic structure and since the three phases considered in the calculations have different electronic structures, the transition to a spin-degenerate state (not shown) is different for them.

The site-projected magnetic moments of the Fe and Mn atoms are displayed in Fig. 8 for the disordered phase and in Fig. 9 for the Mn-pyramidal and Fe-pyramidal phases. For the disordered phase, we observe that for a >5.87 Å all moments are ferromagnetically coupled, but for a <5.87 Å the Mn moment on the tetrahedral site couples antiferromagnetically to the other moments. Notice that the above transition from ferromagnetic to antiferromagnetic coupling occurs at a volume lower than the experimental volume.

The same behavior is actually exhibited by the Fe-pyramidal phase (Fig. 9, squares), where the Mn moment on the tetrahedral site changes from parallel to antiparallel alignment with decreasing volume. However, for the Mn-pyramidal phase the moments are always ferromagnetically aligned (Fig. 9, circles). This phase corresponds to Mn atoms occupying the high-moment site, with Mn moments approaching 3 μ_B/atom. In the Fe-pyramidal phases the Mn moments are always lower than in the Mn-pyramidal phase, and it is tempting to explain the stabilization of the Mn-pyramidal

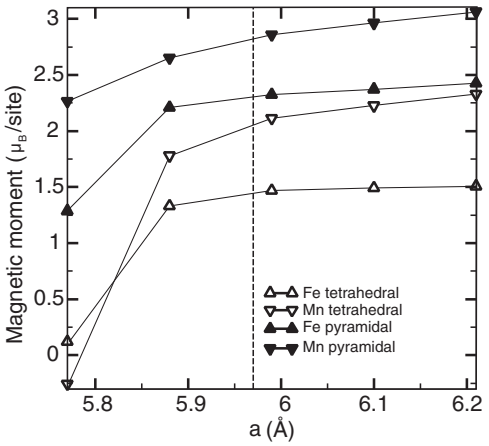

FIG. 8. The site-projected moments of the disordered phases of $FeMnP_{0.75}Si_{0.25}$ as a function of the lattice parameter ($c/a = 0.5894$). The dashed vertical line indicates the experimental a lattice parameter.

phase to be due to the exchange energy of the larger Mn moment in the pyramidal site.

D. Magnetization measurements

Results of magnetization measurements on the quenched sample (C) and slowly cooled sample (D) are shown in Fig. 10. The quenched sample (C) shows a broad para- to ferromagnetic phase transition at approximately 250 K accompanied by strong thermal hysteresis. The observed thermal hysteresis is an indicator of a first-order nature of the phase transition.

The dc susceptibility vs temperature curve for the slowly cooled sample (D) shows a para- to antiferromagnetic phase transition at approximately 160 K. Below the maximum signaling the antiferromagnetic transition at 160 K, the susceptibility slightly increases due to not fully compensated antiferromagnetism. Additionally, there is a significant difference (gap) between the ZFC and FC curves; the irreversibility first appears around 280 K, i.e., well above the Néel temperature, but at a temperature that coincides with the first indications of ferromagnetism in the quenched sample (C). It is also of interest to note that this temperature marks the

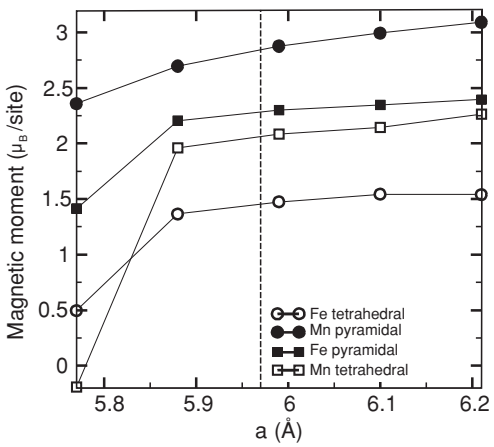

FIG. 9. The site-projected moments of the ordered phases of $FeMnP_{0.75}Si_{0.25}$ as a function of the lattice parameter ($c/a = 0.5894$). The dashed vertical line indicates the experimental a lattice parameter.

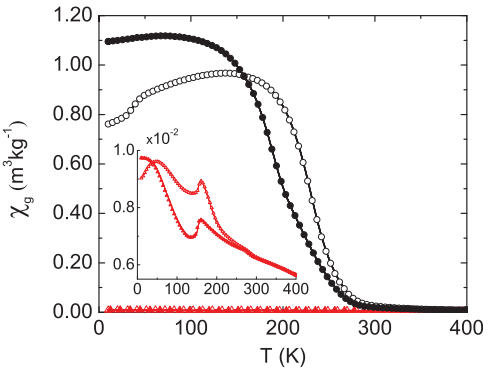

FIG. 10. (Color online) Magnetic susceptibility vs temperature for $FeMnP_{0.75}Si_{0.25}$ measured on the quenched sample in an applied field of ~4 kA/m (black circles) and on the annealed sample under an applied field of ~40 kA/m (red triangles, inset). The open symbols indicate measurements using a zero field cold (ZFC) protocol and the filled symbols using a field cooled (FC) protocol.

onset of a frequency-dependent ac susceptibility that remains frequency-dependent only down to the antiferromagnetic ordering temperature at 160 K. This indicates that clusters of ferromagnetic order start to form around 280 K (the same temperature range in which the quenched sample (C) starts to form a long-ranged ferromagnetic phase). On further cooling global antiferromagnetic interaction forces the sample into long-ranged antiferromagnetic order below about 160 K.

It is worth mentioning that the closely related compound FeMnP (orthorhombic Co_2P structure) also shows an antiferromagnetic structure for 176 K $< T <$ 265 K with a doubling of the crystallographic c axis. Below 175 K a complicated modulated helical antiferromagnetic structure is developed.[27] FeMnP is a fully ordered compound with the tetrahedral Me(I) site and the pyramidal Me(II) site fully occupied by Fe and Mn atoms, respectively.

The magnetization of both samples as a function of the applied field at 30 K is shown in Fig. 11. At an applied field of 3 T the measured magnetic moment is 1.26 μ_B per formula unit (f.u.) for the quenched sample (C) and 0.05 μ_B/f.u. for the slowly cooled sample (D). The figure distinctly pictures the transformation of the low-temperature state of the material

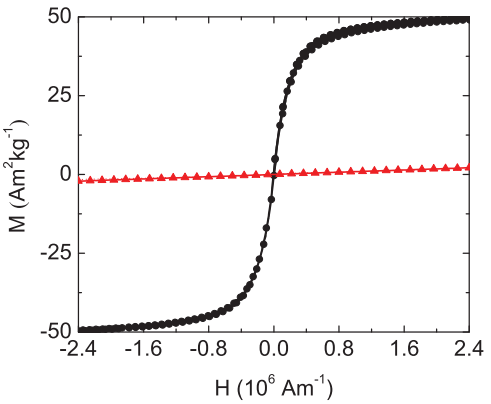

FIG. 11. (Color online) Magnetization vs applied field for a quenched sample at 30 K (black circles) and an annealed sample at 30 K (red triangles).

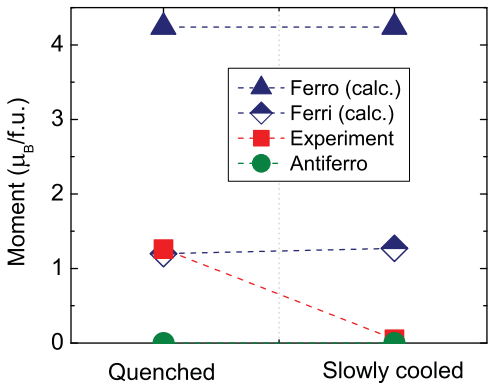

FIG. 12. (Color online) Experimental magnetic moments/f.u. in comparison with calculated moments assuming ferro-, ferri-, and antiferromagnetic ordering.

from ferromagnetic to antiferromagnetic by only an almost marginal change of the site occupancy of the Fe and Mn atoms as observed from the Mössbauer experiments.

In Fig. 12 a comparison between calculated and measured effective magnetic moments is shown. The calculated magnetic moments are obtained by averaging the calculated ordered moments for the Mn-pyramidal, Fe-pyramidal, and disordered phases in proportion to the Fe/Mn ratio and measured disorder from Mössbauer spectroscopy. The ferrimagnetic coupling was assumed to be between the pyramidal and tetrahedral sites. It can be seen that the experimental results for the quenched sample (C) and the slowly cooled sample (D) do not coincide with ferromagnetic ordering. Both the slowly cooled and the quenched samples exhibit more complex magnetic structures such as antiferromagnetism or ferrimagnetism.

In the case of $Fe_{1-x}S$ a rather similar experimental result was explained by the ordering of vacancies on magnetic sublattices, see Takayama *et al.*[28]

IV. SUMMARY AND CONCLUSIONS

In this paper we report on the synthesis and structural characterization of nominal $FeMnP_{0.75}Si_{0.25}$, a compound which crystallizes in the hexagonal Fe_2P-type structure. From the electron probe microanalyzer (WDS-EPMA) and EDS one obtains an actual composition of approximately $Fe_{1.1(1)}Mn_{0.9(1)}P_{0.7(1)}Si_{0.3(1)}$. Two types of samples (quenched and slowly cooled) were synthesized and characterized structurally and magnetically. It is found that marginal changes in the degree of crystallographic order, which eventually may be accompanied by a pnictide element ordering, cause a large change in the magnetic properties.

Slow cooling causes a larger degree of order compared to the rapidly quenched sample, and our analysis from the Mössbauer data suggests that for the slowly cooled sample (D) ∼15(1)% of the pyramidal (high moment) site is occupied by Fe atoms. This corresponds to almost full order for the measured Fe/Mn ratio of ∼1.24. For the quenched sample (C) ∼20(1)% of the pyramidal site is occupied by Fe atoms. Under these assumptions a corresponding redistribution of Mn atoms on the tetrahedral Me(1) site can be estimated to 2% (slowly cooled) and 9% (quenched).

The slowly cooled sample (D), with a higher degree of order, is antiferromagnetic with zero net moment. The quenched sample (C) has a net moment of 1.26 μ_B/f.u. obtained from magnetization measurements. Our experimental finding that the magnetism depends very delicately on the degree of order is in qualitative agreement with the theoretical first-principles results.

The theoretical calculations give rather large magnetic moments for the Fe and Mn atoms, both when occupied on the tetrahedral and pyramidal sites. The largest moment is found for Mn being on the pyramidal site, which reaches values as high as 2.81 μ_B/atom. The theoretical calculated moments for Fe on the pyramidal site (ordered, disordered) = (2.29 μ_B/site, 2.29 μ_B/site) coincide with the average moments obtained from Mössbauer spectroscopy (slowly cooled, quenched) = (1.9 μ_B/site, 2.1 μ_B/site). The calculated moment for Fe located on the tetrahedral sites (1.44 μ_B/site) is significantly larger than that observed by Mössbauer spectroscopy (0.95 μ_B/site).

We do not have experimental values for Mn to compare these theoretical values with, but we can note that normally theory and experiment agree with each other for atomic projected moments of magnetic materials (see, e.g., Ref. 29) with an error being less than 10%. If we assume that this is also the case for the currently studied system, we must conclude that the quenched sample is a ferrimagnet or a noncollinear magnetic structure, possibly involving a spin-spiral state, since a ferromagnetic coupling of the calculated atomic moments would result in a net moment of 4.11 μ_B/f.u., a value much larger than the measured value (see Fig. 12).

The observed magnetic response of $FeMnP_{0.75}Si_{0.25}$ is dependent on the proportion of Fe and Mn atoms occupying the tetrahedral and pyramidal sites. The measured small increase of the Fe concentration on the high-moment pyramidal site, only a few percent, might cause the sample to change from behaving as an antiferromagnet to a ferrimagnet with a rather large saturation moment. A simultaneous decrease of Mn concentration on the tetrahedral site is certainly important for the magnetic interactions and needs to be considered.

It is unclear whether a modification of the stoichiometry would cause a similar change in the magnetic response, but it is tempting to speculate that this may be possible as seen in the case of FeMnP.[9] We also find from our theory that an ordered phase with all Mn atoms on the pyramidal site and all Fe atoms on the tetrahedral site has a significantly lower energy compared to the disordered phase.

The material studied here, $FeMnP_{0.75}Si_{0.25}$, has been characterized structurally and magnetically, with a range of experimental techniques and by first-principles theory, as a member of a family of materials which are relevant for magnetocaloric refrigeration. Our study indicates that the influence of crystallographic order and disorder on the magnetocaloric properties is important and should be studied in more detail. This involves both varying the concentration of Fe and Mn and using different annealing conditions.

ACKNOWLEDGMENTS

Financial support from the Swedish Energy Agency (STEM) and the Swedish Research Council (VR) is ac-

knowledged. Calculations done on supercomputer resources provided by SNAC are acknowledged. O.E. is grateful to the ERC for support. The authors would like to thank Ece Gülşen for the sample fabrication, Rebecca Bejhed, Hans Harrysson, and Hans Annersten for composition analysis, and Roland Mathieu for valuable suggestions and advice.

*matthias.hudl@angstrom.uu.se

[1]E. Brück, O. Tegus, L. Zhang, X. W. Li, F. R. de Boer, and K. H. J. Buschow, J. Alloys Compd. **383**, 32 (2004).
[2]E. Brück, J. Kamarad, V. Sechovsky, Z. Arnold, O. Tegus, and F. de Boer, J. Magn. Magn. Mater. **310**, e1008 (2007).
[3]W. Dagula, O. Tegus, X. W. Li, L. Song, E. Brück, D. T. C. Thanh, F. R. de Boer, and K. H. J. Buschow, J. Appl. Phys. **99**, 08Q105 (2006).
[4]D. T. Cam Thanh, E. Brück, N. T. Trung, J. C. P. Klaasse, K. H. J. Buschow, Z. Q. Ou, O. Tegus, and L. Caron, J. Appl. Phys. **103**, 07B318 (2008).
[5]S. Rundqvist and F. Jellinek, Acta Chem. Scand. **13**, 425 (1959).
[6]R. Wäppling, L. Häggström, T. Ericsson, S. Devanarayanan, E. Karlsson, B. Carlson, and S. Rundqvist, J. Solid State Chem. **13**, 258 (1975).
[7]H. Fujii, T. Hokabe, T. Kamigaichi, and T. Okamoto, J. Phys. Soc. Jpn. **43**, 1 (1977).
[8]L. Lundgren, G. Tarmohamed, O. Beckman, B. Carlsson, and S. Rundqvist, Phys. Scr. **17**, 39 (1978).
[9]B. K. Srivastava, T. Ericsson, L. Häggström, H. R. Verma, Y. Andersson, and S. Rundquist, J. Phys. C. **20**, 463 (1987).
[10]P. Jernberg, A. A. Yousif, L. Häggström, and Y. Andersson, J. Solid State Chem. **53**, 313 (1984).
[11]O. Eriksson, J. Sjöström, B. Johansson, L. Häggström, and H. L. Skriver, J. Magn. Magn. Mater. **74**, 347 (1988).
[12]E. Wohlfarth, J. Appl. Phys. **50**, 7542 (1979).
[13]H. Yamada and K. Terao, Phase Transitions **75**, 231 (2002).
[14]S. Rundqvist, Chem. Scr. **28**, 15 (1988).
[15]O. K. Andersen, O. Jespen, and G. Krier, *Lectures on Methods of Electronic Structure Calculation* (World Scientific, Singapore, 1994).
[16]L. Vitos, H. L. Skriver, B. Johansson, and J. Kollár, Comput. Mater. Sci. **18**, 24 (2000).
[17]L. Vitos, Phys. Rev. B **64**, 014107 (2001).
[18]L. Vitos, *Computational Quantum Mechanics for Materials Engineers: The EMTO Method and Applications* (Springer Verlag, London, 2007).
[19]P. Soven, Phys. Rev. **156**, 809 (1967).
[20]B. L. Györffy, Phys. Rev. B **5**, 2382 (1972).
[21]L. Dubrovinsky, N. Dubrovinskaia, F. Langenhorst, D. Dobson, D. Rubie, C. Geszligmann, I. A. Abrikosov, B. Johansson, V. I. Baykov, L. Vitos *et al.*, Nature **422**, 58 (2003).
[22]J. P. Perdew, K. Burke, and M. Ernzerhof, Phys. Rev. Lett. **77**, 3865 (1996).
[23]J. Kollár, L. Vitos, and H. L. Skriver, *Electronic Structure and Physical Properties of Solids: The Uses of the LMTO Method* (Springer-Verlag, Berlin, 2000).
[24]J. P. Perdew, A. Ruzsinszky, G. I. Csonka, O. A. Vydrov, G. E. Scuseria, L. A. Constantin, X. Zhou, and K. Burke, Phys. Rev. Lett. **100**, 136406 (2008).
[25]B. Carlsson, M. Gölin, and S. Rundqvist, J. Solid State Chem. **8**, 57 (1973).
[26]R. Fruchart, A. Roger, and J. Senateur, J. Appl. Phys. **40**, 1250 (1969).
[27]J. Sjöström, L. Häggström, and T. Sundqvist, Philos. Mag. **57**, 737 (1988).
[28]T. Takayama and H. Takagi, Appl. Phys. Lett. **88**, 012512 (2006).
[29]E. K. Delczeg-Czirjak, L. Delczeg, M. P. J. Punkkinen, B. Johansson, O. Eriksson, and L. Vitos, Phys. Rev. B **82**, 085103 (2010).